NANO LETTERS

xxxx
Vol. 0, No. 0
A−G

Thermal Resistance of Nanoscopic Liquid–Liquid Interfaces: Dependence on Chemistry and Molecular Architecture

Harshit A. Patel,[†] Shekhar Garde,*[,†] and Pawel Keblinski*[,‡]

The Howard P. Isermann Department of Chemical & Biological Engineering and Center for Biotechnology & Interdisciplinary Studies, Rensselaer Polytechnic Institute, Troy, New York 12180, and Materials Science and Engineering Department, Rensselaer Polytechnic Institute, Troy, New York 12180

Received August 3, 2005; Revised Manuscript Received September 17, 2005

ABSTRACT

Systems with nanoscopic features contain a high density of interfaces. Thermal transport in such systems can be governed by the resistance to heat transfer, the Kapitza resistance (R_K), at the interface. Although soft interfaces, such as those between immiscible liquids or between a biomolecule and solvent, are ubiquitous, few studies of thermal transport at such interfaces have been reported. Here we characterize the interfacial conductance, $1/R_K$, of soft interfaces as a function of molecular architecture, chemistry, and the strength of cross-interfacial intermolecular interactions through detailed molecular dynamics simulations. The conductance of various interfaces studied here, for example, water–organic liquid, water–surfactant, surfactant–organic liquid, is relatively high (in the range of 65–370 MW/m^2 K) compared to that for solid–liquid interfaces (∼10 MW/m^2 K). Interestingly, the dependence of interfacial conductance on the chemistry and molecular architecture cannot be explained solely in terms of either bulk property mismatch or the strength of intermolecular attraction between the two phases. The observed trends can be attributed to a combination of strong cross-interface intermolecular interactions and good thermal coupling via soft vibration modes present at liquid–liquid interfaces.

Macroscopic properties of systems with nanoscale features, by their very nature, are dominated by the properties of interfaces. With regards to the transfer of heat, the pioneering work by Kapitza[1] on the resistance of the metal−liquid helium interface has motivated significant research in the area of interfacial heat transfer.[2] Specifically, investigation of the microscopic origin of the so-called Kapitza resistance has been a primary focus of the studies of thermal transport across liquid−solid, and solid−solid interfaces. Fundamental understanding of the Kapitza resistance, R_K, is becoming a technological imperative as well, driven by the recent interest in nanocomposite materials, including ceramics,[3] polymers,[4] and nanofluids[5] that contain a high density of interfaces, and in health applications (e.g., targeted laser-based medical therapies).[6]

Although a substantial body of research exists on the subject of solid−solid and solid−liquid interfacial thermal resistance,[2,7−10] very few studies have focused on liquid−liquid interfaces. The thermal properties of these soft interfaces will be critical in determining heat transfer in biological systems in vivo and in vitro, such as in cellular environments that contain a high density of soft interfaces (e.g., protein−water or lipid membrane−water interfaces) or in protein crystals.

Recent experiments on the thermal relaxation of laser-excited water clusters in a reverse micellar surfactant system[11] and laser-excited metal nanoparticles[12] stabilized with covalently attached surfactant chains provided a measure of the interfacial thermal conductance of hydrophilic interfaces. The thermal relaxation times measured in these experiments are influenced by a number of factors, including the coupling between internal vibrations in molecules and nanoparticles and the heat flow along the surfactant chain. Assuming that the critical step for the relaxation process is heat flow across the solvent−surfactant interface, one obtains a lower bound of interfacial conductance, $G = 1/R_K$, in the range of 100−300 MW/m^2 K for surfactant−water or surfactant−methanol hydrophilic interfaces.[12,13]

In contrast, conductance of an interface between alkanethiol-terminated AuPd nanoparticles and toluene was found to be only 15 MW/m^2 K.[12] If this resistance is attributed to the alkane−toluene interface, then one concludes

* Corresponding authors. E-mail: keblip@rpi.edu; gardes@rpi.edu.
[†] The Howard P. Isermann Department of Chemical & Biological Engineering and Center for Biotechnology & Interdisciplinary Studies.
[‡] Materials Science and Engineering Department.

10.1021/nl051526q CCC: $30.25
Published on Web 00/00/0000

Table 1. Number of Molecules of Each Type and Corresponding Box Dimensions (in Å) Used in MD Simulations of Liquid−Liquid Interfaces

system	water	surfactant	organic	x	y	z
water−octane	800		100	27.7	29.0	66.4
water−benzene	800		120	22.7	24.1	78.4
water−$CH_3(CH_2)_{29}OH$−hexane	824	60	123	28.4	23.3	152.7
water−$CH_3(CH_2)_{29}OH$−benzene	832	60	120	26.5	22.3	151.1

that variation of the molecular interaction strength across the interface can lead to an order of magnitude change in the interfacial thermal resistance.

To investigate the rate and the mechanism of interfacial heat flow and its dependence on the strength of intermolecular interactions, here we employ molecular dynamics (MD) simulations of neat liquid−liquid interfaces. MD simulations allow systematic variation in molecular complexity and intermolecular interactions without being encumbered by interplay between a number of other factors influencing the experimental results.

To understand the effects of cross-interfacial interactions and molecular structures of liquids on the interfacial conductance, we examined heat flow across five model interfaces. Three of these are aqueous interfaces with increasing hydrophilicity from water−octane, to water−benzene, to water−surfactant [$CH_3(CH_2)_{29}OH$] interfaces. We also studied soft organic interfaces between surfactant tails and two organic solvents, benzene and hexane. This was achieved through MD simulations of four distinct setups, water−octane, water−benzene, water−surfactant−hexane, and water−surfactant−benzene systems. Collectively, these systems sample a range of intermolecular interactions as well molecular architectures across soft interfaces.

Our calculations highlight a number of properties that are unique to liquid−liquid interfaces. We show that the heat conductance ($1/R_K$) of soft liquid−liquid interfaces is relatively high compared to solid−liquid interfaces. More interestingly, the dependence of interfacial conductance on the chemistry and molecular architecture of phases cannot be explained solely in terms of either bulk property mismatch or the strength of the intermolecular attraction between the two phases. A combined framework that includes the bulk properties of interacting liquids as well as the strength of interfacial coupling is needed for the quantitative prediction of interfacial resistance. Our calculations represent a first step in that direction using molecular simulations of model interfaces.

MD simulations were performed with periodic boundary conditions applied in all three directions. As a result, water−octane and water−benzene systems contain two similar but separate water−organic liquid interfaces. Thirty C30-alkanol [$CH_3(CH_2)_{29}OH$] surfactant molecules were added at each of these interfaces so that these new systems contained two distinct water−surfactant (headgroup) as well as two distinct organic−liquid-surfactant (tailgroup) interfaces. Two different organic liquids, hexane (instead of octane) and benzene, were used in these additional MD simulations.

Table 1 lists the dimensions of all of the systems and the number of molecules simulated here. The length of water−octane and water−benzene systems in the direction perpendicular to interfaces (z direction) is about 70 Å, with the thickness of each slab being about 35 Å (Figure 1A). The corresponding size of the surfactant systems is larger (∼150 Å) because of the presence of two surfactant layers (see Figure 2A). The lateral sizes (x and y) are about 25 Å for all structures.

All atoms were represented explicitly in MD simulations. Water molecules were represented by the three-point charge TIP3P model,[14] whereas hydrocarbons and surfactant molecules were represented using the all-atom AMBER force field that includes bond length, bond angle, torsion, and nonbonded Lennard−Jones and Coulomb terms.[15] Benzene molecules were represented using the Jorgensen and Severance[16] model modified to reproduce the experimental density

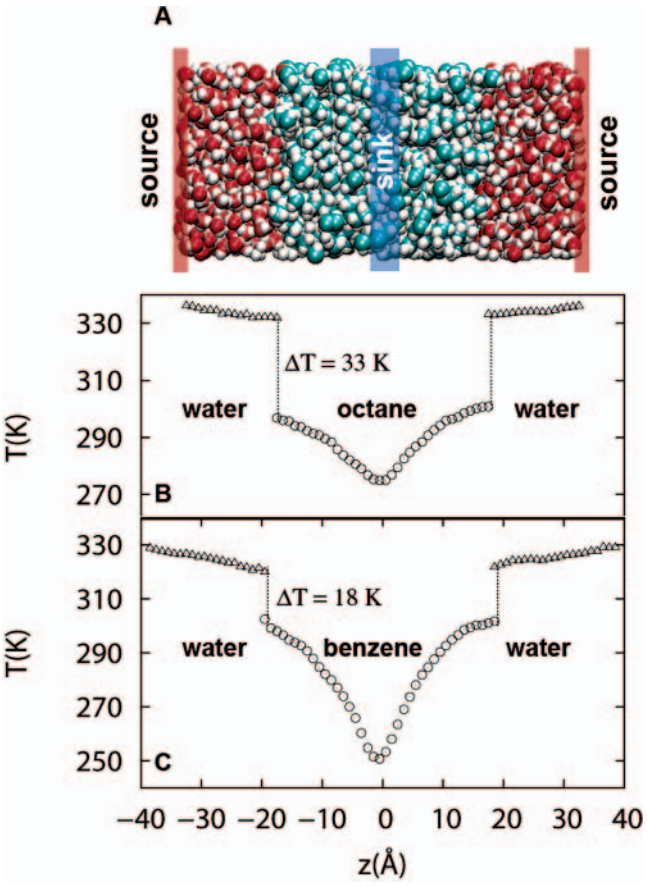

Figure 1. (Panel A) Molecular dynamics snapshot of the water−octane system shown using a spacefilling representation: oxygens (red), hydrogens (white), and carbons of octane (cyan). Heat source and sink regions are identified schematically with red and blue vertical stripes, respectively. Panels B and C show the steady-state temperature profiles in the water−octane and water−benzene systems, respectively. ΔT is the temperature drop at the interface.

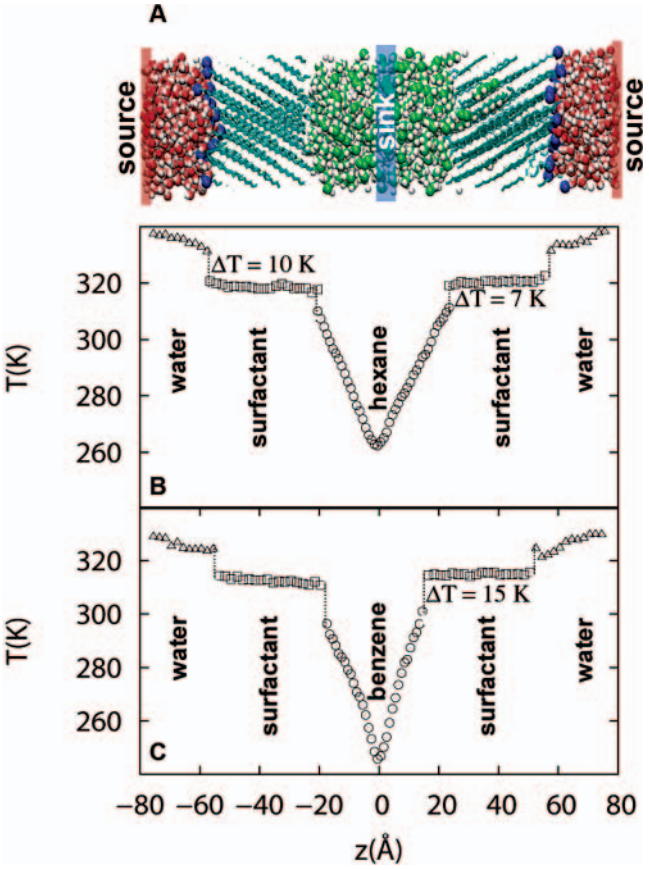

Figure 2. (Panel A) Molecular dynamics snapshot of the water−surfactant−hexane system shown using a spacefilling representation: oxygens (red), hydrogens (white), carbons of hexane (green), surfactant tails (cyan), and headgroup oxygens (blue). Heat source and sink regions are identified schematically with red and blue vertical stripes, respectively. Panels B and C show the steady-state temperature profiles in the water−surfactant−hexane and water−surfactant−benzene systems, respectively. ΔT is the temperature drop at the interface.

at 1 atm.[17] Bond vibrations were simulated without constraints. The particle mesh Ewald method[18] with a grid spacing of approximately 1 Å was used to calculate electrostatic interactions. Constant NPT (1 atm, 300 K) simulations were carried out during equilibration with a 2-fs time step and using Berendsen baro- and thermostats.[19]

Following equilibration, we conducted MD simulations in the microcanonical (NVE) ensemble with a shorter time step (1 fs) to ensure energy conservation. We defined two 5-Å-thick slabs, one as a heat source and the other as a heat sink located at the center of the water and organic liquid phases, respectively (see Figure 1A). Atomic velocities were scaled up (down) in the heat source (sink) regions so that heat was added at a constant rate of dQ/dt to the source and removed at the same rate from the sink.[20] Care was taken to ensure both total energy and momentum conservation during the velocity scaling procedure.[21] We monitored the temperature profile along the z direction by calculating the total kinetic energy of the atoms in 1-Å slices in each phase. For dQ/dt $= 3.45 \times 10^{-8}$ J/s, the value selected here, a steady-state temperature profile is established in ∼500 ps. MD simulations were run for an additional 1 ns after a steady state is established.

The method of using a heat source and a sink in MD simulations is now well established.[20,22−24] To test our implementation of the method, we calculated thermal conductivities (κ) of pure water, octane, and benzene liquids by performing independent MD simulations of these liquids. We obtain κ using Fourier's law

$$j_Q = -\kappa \frac{\partial T}{\partial z} \tag{1}$$

where $j_Q = (\mathrm{d}Q/\mathrm{d}t)/2A$ is the heat flux, A is the cross-sectional area (the factor of 2 accounts for heat flow in both positive and negative z-directions in periodic systems), and $\partial T/\partial z$ is the slope of the steady-state temperature profile. We find $\kappa = 0.7$ W/m K for water, which compares well with the experimental value of 0.61 W/m K,[25] as well as with the value reported for other similar water models (∼0.73 W/m K).[22]

The thermal conductivities for organic liquids obtained from our simulations, 0.16 W/m K for octane and 0.08 W/m K for benzene, are significantly lower than that for water, again in excellent agreement with experimental data. The numerical values of κ for octane and benzene are similar to but not in precise quantitative agreement with experiments. For example, model octane is more thermally conductive than benzene, whereas experiments show the opposite trend with $\kappa_{\mathrm{octane}} = 0.12$ W/m K[26] and $\kappa_{\mathrm{benzene}} = 0.14$ W/m K,[27] respectively. Overall, the simulation models indeed capture the large differences in conductivities between water and organic liquids, with the largest numerical discrepancy observed for liquid benzene. Although the quantitative discrepancy could be overcome by development of better force fields, the present models clearly capture thermal conductivity differences between strongly self-associating fluid (water) and nonassociating organic liquids. Further interfacial molecular structure is also captured sufficiently accurately, which allows characterization of the effect of cross-interfacial intermolecular interactions (e.g., hydrophobic/hydrophilic) and molecular architecture on thermal transport.

Figure 1B shows the steady-state temperature profile for the water−octane system. Temperature drops monotonically from ∼335 K at the heat source located at the center of the water phase to ∼275 K at the center of the octane phase, where the heat sink is located. The temperature drop is smaller in water compared to that in octane, consistent with the higher thermal conductivity of water relative to octane. Further, temperature profiles in both water and octane phases are continuous but nonlinear. This is in contrast to the profiles observed in simulations of pure liquids from our group (not shown) as well as others,[20,22−24] which appear perfectly linear. Therefore, the nonlinear nature of the temperature profile results primarily from the presence of the interface. It is known that the packing and orientations of water and octane molecules at the interface show systematic differences in the ∼1-nm-wide interfacial region compared to that in the bulk phase.[28−30] The interface is also not perfectly flat and shows

Table 2. Interfacial Thermal Conductance and Equivalent Liquid Thickness for Water Calculated for the Five Different Interfaces Simulated Here

interface	G (MW/m^2 K)	h_{water} (nm)
water−octane	65 ± 10	10.7
water−benzene	175 ± 25	4.0
water−surfactant head	300 ± 40	2.7
hexane−surfactant tail	370 ± 40	1.9
benzene−surfactant tail	200 ± 30	3.6

roughness on the molecular lengthscales. Clearly, the inhomogeneous nature of the interface affects the local environment so that the slope of the measured temperature profile is smaller near the interface than that in the bulk for both octane and water.

Most notably, there is a large temperature discontinuity, ΔT (~33 K), at the water−octane interface. This gives an estimate of the interfacial conductance, $G = -j_Q/\Delta T$, to be 65 ± 10 MW/m^2 K for that interface. This value can be interpreted alternatively in terms an "equivalent liquid thickness", $h = \kappa/G$, which is the thickness of the liquid phase over which the temperature drop is equal to ΔT for a given flux, j_Q. $G_{water-octane} = 65$ MW/m^2 K gives $h_{water} = 10.7$ nm and $h_{octane} = 2.5$ nm. Thus, for nanoscopic structures involving interfaces separated by 10-nm-thick slabs of liquids or less, the interfacial resistance will be important, and in some cases even a dominant factor in determining the overall heat flow.

Table 2 lists the interfacial conductances obtained similarly using temperature drops at other interfaces. In general, all of the conductances measured here between soft interfaces are relatively high, ranging from 65 to 370 MW/m^2 K. The trend in these values with changing intermolecular interactions and molecular architecture is, however, interesting. For example, for aqueous interfaces, the conductance of the water−benzene interface is higher than that of the water−octane interface, and that of the water−surfactant headgroup interface is even higher.

This trend can be attributed to the strength of interfacial coupling of water molecules with molecules of the other fluid through stronger intermolecular interactions. Indeed, the atomic sites of benzene have higher partial charges compared to those of octane. The relatively more favorable solvation of benzene compared to that of octane is also reflected in the orders of magnitude higher saturation solubility of benzene in water relative to octane.[31] The overall mass density profiles also show a higher density of benzene molecules at the aqueous interface compared to that of octane (see Figure 3A). In addition, the similarity between the more compact and rigid molecular structures of water and benzene molecules compared to that between water and the more flexible octane molecules might lead to a better coupling between the water and benzene phases.

The large conductance of the water−surfactant headgroup interface (~300 MW/m^2 K) is due primarily to the strong coupling through hydrogen bonding of water molecules with the hydroxyl headgroups of surfactant molecules. The surfactant headgroups are dipolar, and therefore, strongly solvated by vicinal water molecules. Figure 3C shows that the hydroxyl headgroups of surfactant molecules accept as well as donate hydrogen bonds to the vicinal water molecules. This favorable interaction leads to a visible peak in the overall mass density profile at the surfactant headgroup−water interface as shown in Figure 3D, consistent with the interpretation of electron density profiles obtained for an identical interface using X-ray reflectivity experiments.[32]

Interestingly, Figure 2 (panels B and C) shows that there is very little temperature drop along the entire length of surfactant chains. This can be understood by focusing on the conformations of surfactant tails. X-ray reflectivity experiments for a similar system show perfect crystalline organization of surfactants at the water−vapor interface.[32] At the liquid−liquid water−hexane interface, although the chains are densely packed, there is penetration of the hexane molecules in the tail region leading to more disordered structures.[32] Over the time scale of our simulations, we do observe some penetration of hexane molecules in the tail region (see Figure 3B and E), although most surfactant chains are predominantly straight (Figure 2A). The thermal vibration waves (phonons) can propagate along such straight and densely packed chains with great efficiency, leading to excellent heat conduction. In fact, a similar mechanism is responsible for an orders of magnitude increase in the thermal conductivity of polyethylene upon drawing.[33] A larger thermal resistance is expected for the heat flow through structures made of less-ordered unsaturated, kinked surfactant chains or through membranes comprising double-tailed lipid molecules.

Table 2 shows that the interfaces of organic liquids with surfactant tailgroups are highly conductive. The hexane−surfactant tailgroup interfaces have the highest thermal conductance (~370 MW/m^2 K). This is surprising because the strength of the intermolecular interactions between hexane and surfactant tails are similar to those between octane and water. The large conductance of the hexane−surfactant interface could be explained partly by the penetration of a hexane molecule observed in our simulations (Figure 3B and E) as well as in experiments. In contrast, we do not observe any penetration of surfactant tail regions by benzene molecules (Figure 3B). Correspondingly, replacing hexane with benzene reduces the interfacial conductance significantly to 200 MW/m^2 K. Further, the higher conductance of the hexane−surfactant interface may also be associated with very similar molecular and thus vibrational structures of the hydrocarbon surfactant tails and the hexane molecules. In general, more pronounced dissimilarities between molecular structures of the two liquids forming the interface will lead to larger interfacial thermal resistance.

The theoretical framework for understanding the interfacial heat flow for solid−solid and solid−liquid interfaces is provided by the "acoustic mismatch model" (AMM) and the "diffusive mismatch model" (DMM).[2] Both models consider the transmission and reflection of propagating heat waves (phonons) at an interface. In the AMM, the transmission and reflection coefficients for phonons are given by classical wave propagation formulas, whereas the (DMM) assumes that all phonons striking the interface are scattered to one of

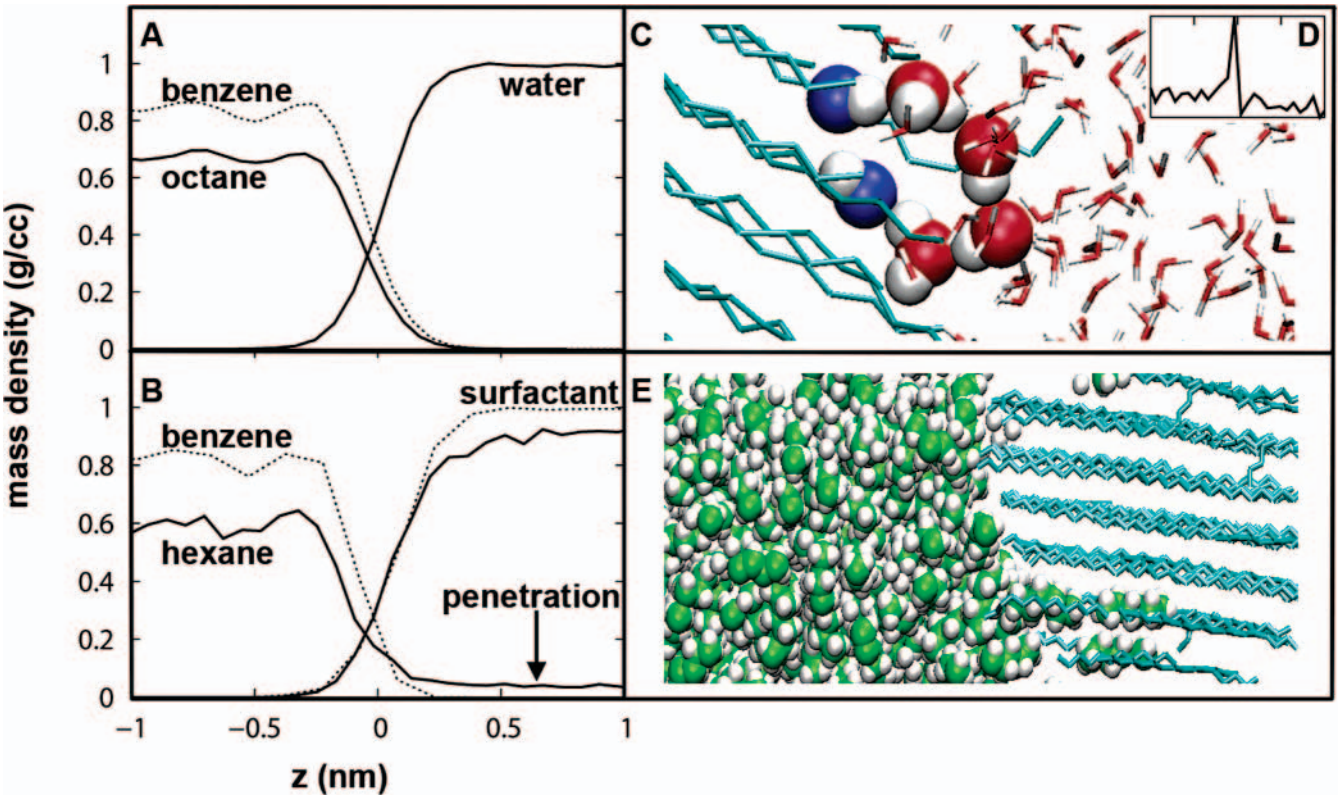

Figure 3. (Panel A) Interfacial mass density profile of water, octane, and benzene molecules at the water−octane and water−benzene interfaces, respectively. (Panel B) Similar to A for benzene and hexane at the surfactant tail interface. Penetration of hexane molecules into the tail region is clearly observed. The surfactant tail density drops and the profile becomes less sharp in this case. Hexane penetration is also visible in the MD snapshot of the tail region (panel E, hexane (green and white) and tails (cyan)). Panel C shows hydrogen bonding between water molecules (oxygen (red) and hydrogen (white)) and selected hydroxyl headgroups of surfactants (oxygen (blue) and hydrogen (white)). The corresponding peak in the interfacial mass density is shown in panel D in arbitrary units.

the adjoining phases with a probability that is proportional to the phonon density of states in this substance. For liquid−liquid interfaces, both AMM and DMM are not directly applicable because neither phase involved is a solid; thus, there are no propagating phonons.

Nevertheless, to gain a more detailed understanding of the heat flow across liquid−liquid interfaces, we analyze the vibrational characteristic of liquids forming interfaces. This is achieved by first calculating the velocity autocorrelation function, VAF $= \langle v(t)v(0)\rangle$, where v is the velocity of a heavy atom (e.g., an oxygen atom in a water molecule), t is time, and $\langle\ \rangle$ denotes the ensemble average. The Fourier transform of the VAF provides the so-called vibrational density of states (VDOS), which represents the spectral description of the atomic and molecular motions in liquids.

The VDOS for all of the liquids studied here as well as for the head and tail groups of the surfactant molecules are shown in Figure 4. In all cases, only low frequency parts of the vibrational spectra are shown because they represent modes responsible for carrying heat from one molecule to another. High-frequency, intramolecular motions associated with covalent bond vibrations do not contribute significantly to intermolecular thermal transport because those modes are localized on individual molecules.

All of the liquids studied here exhibit a broad low-frequency peak in VDOS associated with intermolecular motions governed by nonbonded interactions (van der Waals and electrostatic). That peak in water is located at higher frequencies compared to that in hydrocarbon liquids because of stronger electrostatic interactions between water molecules. The peaks for surfactant head and tail groups are also located at relatively high frequencies; this is most likely associated with the more ordered structure of the surfactant.

Although it is very difficult to obtain a quantitative relationship between the VDOS profiles and the interfacial thermal conductance, the extent of overlap between the VDOS profiles of two different phases forming an interface can be taken as a qualitative measure of vibrational coupling. Higher overlap could allow more efficient heat flow through such "harmonic" coupling.

Indeed, recent combined experimental and atomistic simulation work showed a rather small interfacial thermal conductance between single-walled carbon nanotubes suspended in surfactant micelles in water[34] and between C84 fullerene and organic solvents, equal to 10−20 MW/m^2 K.[35] This low conductance can be explained partly by focusing on the overlap of corresponding VDOS profiles. As shown in Figure 4D, the low-frequency regions of the VDOS of a model C_{84} molecule and octane liquid have essentially no overlap between them.[35] This leaves only the nonharmonic thermal coupling between C_{84} and octane that does not provide an efficient mechanism for the transport of thermal energy, giving a low value of $G_{C84-octane} \approx 10$ MW/m^2 K measured in both experiment and simulations. In contrast,

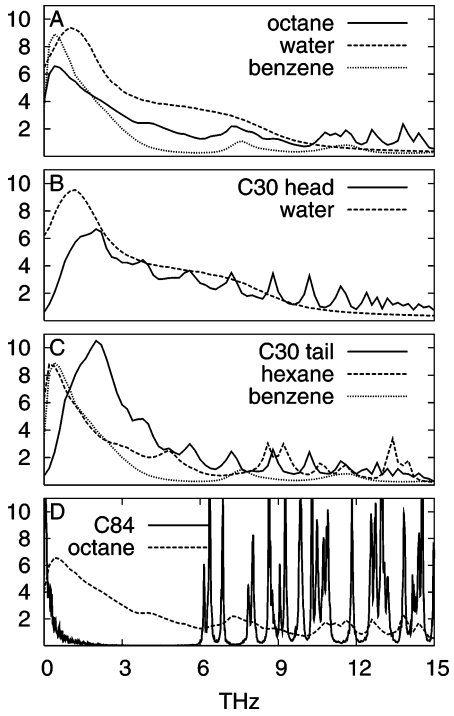

Figure 4. (Panels A through C) Fourier transforms of the velocity autocorrelation functions of the heavy atoms for each phase shown in Figures 1 and 2. Panel D shows the Fourier transform of the velocity autocorrelation function for a C84 molecule in liquid octane and for the octane solvent.[35]

the VDOS profiles of the liquids studied here exhibit a broad peak in the low-frequency region, which allows for significant overlap, the extent of which depends on the specific liquid pair being considered. As a result, interfacial thermal conductances of all of the interfaces studied here are relatively high, on the order of 100 MW/m^2 K or higher.

We presented calculations of interfacial heat conductance for several model soft (liquid−liquid) interfaces with varying chemistry and molecular architecture. Overall, the conductances of these soft interfaces are relatively high, of the order of 100 MW/m^2 K. This indicates that the low conductance (∼15 MW/m^2 K) between surfactant stabilized nanoparticles and toluene measured in experiments[12] arises not from the poor thermal coupling between surfacant and toluene interface but from elsewhere (e.g., nanoparticle−surfactant bonding, or the disorder in surfactant tails).

The numerical value of the conductance of a given surface characterizes the extent of interfacial (thermal) coupling between the two phases. That coupling is expected to depend on the mismatch between bulk properties of those phases as well as on the strength of the intermolecular attraction between the molecules of the two phases. To characterize the former, we used used vibrational density of states (VDOS) profiles and the extent of their overlap as a qualitative measurement of thermal conductance. We note, however, that the VDOS profile for a given liquid essentially takes into account properties of that fluid alone and misses the information about "interfacial coupling" with the other phase. That coupling is characterized qualitatively by various measures of interfaces (e.g., density profiles, surface tension, etc.). A combined framework that includes the properties of individual liquids (such as VDOS) and some measure of interfacial coupling will be needed for quantitative prediction of interfacial conductances. Molecular dynamics simulations can play an important role in developing such a framework by providing clean results for model systems with increasing complexity.

Finally, we comment on the issue of thermal conductance between water and biomolecules. The thermal conductivities of biomolecules and their secondary structural components have been studied recently.[36,37] Considering that surfaces of proteins, DNA, and other biomolecules can be viewed as a mixture of hydrophobic and hydrophilic sites, one can expect $G_{\text{biomolecule-water}} \approx 100$ MW/m^2 K, with an equivalent water thermal resistance thickness, $h \approx 5$ nm. This resistance might be a significant factor limiting heat flow in typical biological environments that contain a high density of interfaces.

Acknowledgment. We thank the NSF Nanoscale Science and Engineering Center for Directed Assembly of Nanostructures (DMR) for partial financial support of the work. S.G. and P.K. also gratefully acknowledge financial support of the NSF CAREER awards, CTS-0134023 and DMR-134725.

References

(1) Kapitza, P. L. *Zh. Eksp. Teor. Fiz.* **1941**, *4*, 181.
(2) Swartz, E. T.; Pohl, R. O. *Rev. Mod. Phys.* **1989**, *61*, 605.
(3) Siegel, R. W.; Chang, S. K.; Ash, B. J.; Stone, J.; Ajayan, P. M.; Doremus, R. W.; Schadler, L. S. *Scr. Mater.* **2001**, *44*, 2061−2064.
(4) Becker, C, Krug, H.; Schmidt, H. *Mater. Res. Soc. Symp. Proc.* **1996**, *435*, 237.
(5) Choi, S. *ASME* **1995**, *66*, 99.
(6) Hirsch, L. R.; Stafford, R. J.; Bankson, J. A.; Sershen, S. R.; Rivera, B.; Price, R. E.; Hazle, J. D.; Halas, N. J.; West, J. L. *Proc. Natl. Acad. Sci. U.S.A.* **2003**, *23*, 13549.
(7) Cahill, D. G.; Ford, W. K.; Goodson, K. E.; Mahan, G. D.; Majumdar, A.; Maris, H. J.; Merlin, R.; Phillpot, S. R. *Appl. Phys. Rev.* **2003**, *93*, 793.
(8) Xue, L.; Keblinski, P.; Phillpot, S.; Choi, S.; Eastman, J. *J. Chem. Phys.* **2003**, *118*, 337.
(9) Barrat, J.-L.; Chiaruttini, F. *Mol. Phys.* **2003**, *101*, 1605.
(10) Graebner, J.; Jin, S.; Kammolott, G.; Herb, J.; Gardinier, F. *Nature* **1992**, *359*, 401.
(11) Deak, J. C.; Pang, Y. S.; Sechler, T. D.; Wang, Z. H.; Dlottt, D. D. *Science* **2004**, *306*, 473.
(12) Ge, Z. B.; Cahill, D. G.; Braun, P. V. *J. Phys. Chem. B* **2004**, *108*, 18870−18875.
(13) Plech, A.; Kotaidis, V.; Gresillon, S.; Dahmen, C.; von Plessen, G. *Phys. Rev. B* **2004**, *70*, -.
(14) Jorgensen, W. L.; Tirado-Rives, J. *J. Am. Chem. Soc.* **1988**, *110*, 1657−1666.
(15) Cornell, W. D.; Cieplak, P.; Bayly, C. I.; Gould, I. R.; Merz, K. M.; Ferguson, D. M.; Spellmeyer, D. C.; Fox, T.; Caldwell, J. W.; Kollman, P. A. *J. Am. Chem. Soc.* **1995**, *117*, 5179−5197.
(16) Jorgensen, W. L.; Severance, D. L. *J. Am. Chem. Soc.* **1990**, *112*, 4768−4774.
(17) MullerPlathe, F. *Macromolecules* **1996**, *29*, 4782−4791.
(18) Darden, T.; York, D.; Pedersen, L. *J. Chem. Phys.* **1993**, *98*, 10089−10092.
(19) Berendsen, H. J. C.; Postma, J. P. M.; van Gunsteren, W. F.; DiNola, A.; Haak, J. R. *J. Chem. Phys* **1984**, *81*, 3684−3690.
(20) MullerPlathe, F. *J. Chem. Phys.* **1997**, *106*, 6082.
(21) Jund, P.; Jullien, R. *Phys. Rev. B* **1999**, *59*, 13707−13711.
(22) Bedrov, D.; Smith, G. D. *J. Chem. Phys.* **2000**, *113*, 8080.
(23) Osman, M. A.; Srivastava, D. *Nanotechnology* **2001**, *12*, 21.
(24) Chantrenne, P.; Barrat, J.-L. *J. Heat Transfer* **2004**, *126*, 577.
(25) Ramires, M. L. V.; Decastro, C. A. N.; Nagasaka, Y.; Nagashima, A.; Assael, M. J.; Wakeham, W. A. *J. Phys. Chem. Ref. Data* **1995**, *24*, 1377−1381.

(26) Watanabe, H.; Seong, D. J. *Int. J. Thermophys.* **2002**, *23*, 337−356.
(27) Assael, M. J.; Ramires, M. L. V.; Decastro, C. A. N.; Wakeham, W. A. *J. Phys. Chem. Ref. Data* **1990**, *19*, 113−117.
(28) Patel, H. A.; Nauman, E. B.; Garde, S. *J. Chem. Phys.* **2003**, *119*, 9199.
(29) Pohorille, A.; Wilson, M. A. *J. Chem. Phys.* **1996**, *104*, 3760−3773.
(30) Pratt, L. R.; Pohorille, A. *Chem. Rev.* **2002**, *102*, 2671−2691.
(31) Lide, D. R. *CRC Handbook of Chemistry and Physics*; CRC Press: Boca Raton, FL, 2005.
(32) Tikhonov, A. M.; Pingali, S. V.; Schlossman, M. L. *J. Chem. Phys.* **2004**, *120*, 11822.
(33) Choy, C. L.; Luk, W. H.; Chen, F. C. *Polymer* **1978**, *19*, 155.
(34) Huxtable, S. T.; Cahill, D. G.; Shenogin, S.; Xue, L. P.; Ozisik, R.; Barone, P.; Usrey, M.; Strano, M. S.; Siddons, G.; Shim, M.; Keblinski, P. *Nat. Mater.* **2003**, *2*, 731−734.
(35) Huxtable, S. T.; Cahill, D. G.; Shenogin, S.; Keblinski, P. *Chem. Phys. Lett.* **2005**, *407*, 129.
(36) Yu, X.; Leitner, D. M. *J. Chem. Phys.* **2005**, *122*, 054902.
(37) Leitner, D. M. *Phys. Rev. Lett.* **2005**, *87*, 188102-1.

NL051526Q